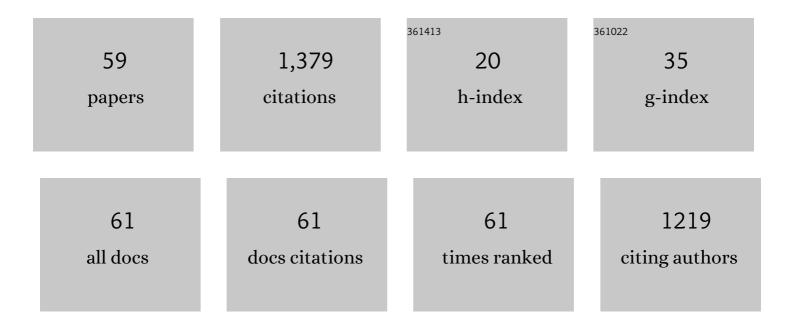
## Chao Zhang

List of Publications by Year in descending order

Source: https://exaly.com/author-pdf/966381/publications.pdf Version: 2024-02-01



#	Article	IF	CITATIONS
1	Tracing the evolution and distribution of F and Cl in plutonic systems from volatile-bearing minerals: a case study from the Liujiawa pluton (Dabie orogen, China). Contributions To Mineralogy and Petrology, 2012, 164, 859-879.	3.1	94
2	Timing and genesis of the adakitic and shoshonitic intrusions in the Laoniushan complex, southern margin of the North China Craton: Implications for post-collisional magmatism associated with the Qinling Orogen. Lithos, 2011, 126, 212-232.	1.4	93
3	Constraints from experimental melting of amphibolite on the depth of formation of garnet-rich restites, and implications for models of Early Archean crustal growth. Precambrian Research, 2013, 231, 206-217.	2.7	84
4	Genesis of leucogranite by prolonged fractional crystallization: A case study of the Mufushan complex, South China. Lithos, 2014, 206-207, 147-163.	1.4	79
5	Origin of high-Mg adakitic magmatic enclaves from the Meichuan pluton, southern Dabie orogen (central China): Implications for delamination of the lower continental crust and melt-mantle interaction. Lithos, 2010, 119, 467-484.	1.4	75
6	Halogen geochemistry of I- and A-type granites from Jiuhuashan region (South China): Insights into the elevated fluorine in A-type granite. Chemical Geology, 2018, 478, 164-182.	3.3	70
7	New Lu–Hf geochronology constrains the onset of continental subduction in the Dabie orogen. Lithos, 2011, 121, 41-54.	1.4	54
8	Zircon U–Pb age, Hf isotopic compositions and geochemistry of the Silurian Fengdingshan I-type granite Pluton and Taoyuan mafic–felsic Complex at the southeastern margin of the Yangtze Block. Journal of Asian Earth Sciences, 2013, 74, 11-24.	2.3	47
9	Mineralogical and geochemical constraints on contribution of magma mixing and fractional crystallization to high-Mg adakite-like diorites in eastern Dabie orogen, East China. Lithos, 2013, 172-173, 118-138.	1.4	42
10	A Practical Method for Accurate Measurement of Trace Level Fluorine in Mg―and Feâ€Bearing Minerals and Glasses Using Electron Probe Microanalysis. Geostandards and Geoanalytical Research, 2016, 40, 351-363.	3.1	41
11	Early Jurassic mafic dykes from the Xiazhuang ore district (South China): Implications for tectonic evolution and uranium metallogenesis. Lithos, 2015, 239, 71-85.	1.4	40
12	Implications of subduction and subduction zoneÂmigration of the Paleo-Pacific Plate beneath eastern North China, based on distribution, geochronology, and geochemistry of Late Mesozoic volcanic rocks. International Journal of Earth Sciences, 2011, 100, 1665-1684.	1.8	38
13	Calculating biotite formula from electron microprobe analysis data using a machine learning method based on principal components regression. Lithos, 2020, 356-357, 105371.	1.4	36
14	Ti-in-quartz thermobarometry and TiO2 solubility in rhyolitic melts: New experiments and parametrization. Earth and Planetary Science Letters, 2020, 538, 116213.	4.4	36
15	Isotopic Compositions (Liâ€Bâ€Siâ€Oâ€Mgâ€Srâ€Ndâ€Hfâ€Pb) and Fe <sup>2+</sup> /ΣFe Ratios of Three Syr Glass Reference Materials (ARMâ€1, ARMâ€2, ARMâ€3). Geostandards and Geoanalytical Research, 2021, 45, 719-745.	nthetic And 3.1	desite 32
16	Anatexis at the roof of an oceanic magma chamber at IODP Site 1256 (equatorial Pacific): an experimental study. Contributions To Mineralogy and Petrology, 2015, 169, 1.	3.1	29
17	The Formation of Tonalites–Trondjhemite–Granodiorites in Early Continental Crust. , 2019, , 133-168.		29
18	Petrogenesis and tectonic implications of A-type granites in the Dabie orogenic belt, China: geochronological and geochemical constraints. Geological Magazine, 2009, 146, 638-651.	1.5	26

CHAO ZHANG

#	Article	IF	CITATIONS
19	Water-enhanced interdiffusion of major elements between natural shoshonite and high-K rhyolite melts. Chemical Geology, 2017, 466, 86-101.	3.3	24
20	Calculating amphibole formula from electron microprobe analysis data using a machine learning method based on principal components regression. Lithos, 2020, 362-363, 105469.	1.4	23
21	Felsic Plutonic Rocks from IODP Hole 1256D, Eastern Pacific: Implications for the Nature of the Axial Melt Lens at Fast-Spreading Mid-Ocean Ridges. Journal of Petrology, 2017, 58, 1535-1565.	2.8	20
22	Electron microprobe technique for the determination of iron oxidation state in silicate glasses. American Mineralogist, 2018, 103, 1445-1454.	1.9	20
23	Apatite in the dike-gabbro transition zone of mid-ocean ridge: Evidence for brine assimilation by axial melt lens. American Mineralogist, 2017, 102, 558-570.	1.9	19
24	Rapid cooling history of a Neotethyan ophiolite: Evidence for contemporaneous subduction initiation and metamorphic sole formation. Bulletin of the Geological Society of America, 2019, 131, 2011-2038.	3.3	19
25	Trace element evidence for anatexis at oceanic magma chamber roofs and the role of partial melts for contamination of fresh MORB. Lithos, 2016, 260, 1-8.	1.4	18
26	Significant boron isotopic fractionation in the magmatic evolution of Himalayan leucogranite recorded in multiple generations of tourmaline. Chemical Geology, 2021, 571, 120194.	3.3	18
27	Rapid hydrothermal cooling above the axial melt lens at fast-spreading mid-ocean ridge. Scientific Reports, 2014, 4, 6342.	3.3	17
28	Boron isotopes in boninites document rapid changes in slab inputs during subduction initiation. Nature Communications, 2022, 13, 993.	12.8	17
29	Stabilizing Perovskite Structure by Interdiffusional Tailoring and Its Application in Composite Mixed Oxygenâ€Ionic and Electronic Conductors. Angewandte Chemie - International Edition, 2017, 56, 7584-7588.	13.8	16
30	Volatiles (CO2, S, F, Cl, Br) in the dike-gabbro transition zone at IODP Hole 1256D: Magmatic imprint versus hydrothermal influence at fast-spreading mid-ocean ridge. Chemical Geology, 2017, 459, 43-60.	3.3	16
31	Chlorine-rich amphibole in deep layered gabbros as evidence for brine/rock interaction in the lower oceanic crust: A case study from the Wadi Wariyah, Samail Ophiolite, Sultanate of Oman. Lithos, 2018, 323, 125-136.	1.4	16
32	Experiments on the Saturation of Fluorite in Magmatic Systems: Implications for Maximum F Concentration and Fluorine-Cation Bonding in Silicate Melt. Journal of Earth Science (Wuhan, China), 2020, 31, 456-467.	3.2	16
33	Decompressional anatexis in the migmatite core complex of northern Dabie orogen, eastern China: Petrological evidence and Ti-in-quartz thermobarometry. Lithos, 2014, 202-203, 227-236.	1.4	14
34	Electron probe microanalysis of Fe2+/ΣFe ratios in calcic and sodic-calcic amphibole and biotite using the flank method. Chemical Geology, 2019, 509, 152-162.	3.3	14
35	Geochronology and geochemistry of the Early Cretaceous Jigongshan and Qijianfeng batholiths in the Tongbai orogen, central China: implications for lower crustal delamination. International Journal of Earth Sciences, 2013, 102, 1045-1067.	1.8	13
36	Electron Probe Microanalysis of Bromine in Minerals and Glasses with Correction for Spectral Interference from Aluminium, and Comparison with Microbeam Synchrotron Xâ€Ray Fluorescence Spectrometry. Geostandards and Geoanalytical Research, 2017, 41, 449-457.	3.1	13

CHAO ZHANG

#	Article	IF	CITATIONS
37	Mafic dykes derived from Early Cretaceous depleted mantle beneath the Dabie orogenic belt: implications for changing lithosphere mantle beneath Eastern China. Geological Journal, 2011, 46, 333-343.	1.3	12
38	The magma plumbing system of Mesozoic Shanyang porphyry groups, South Qinling and implications for porphyry copper mineralization. Earth and Planetary Science Letters, 2020, 543, 116346.	4.4	12
39	GeoBalance: An Excel VBA program for mass balance calculation in geosciences. Chemie Der Erde, 2020, 80, 125629.	2.0	11
40	Multi‣tage Hydrothermal Veins in Layered Gabbro of the Oman Ophiolite: Implications for Focused Fluid Circulation in the Lower Oceanic Crust. Journal of Geophysical Research: Solid Earth, 2021, 126, e2021JB022349.	3.4	9
41	Origin and evolution of ultrapotassic intermediate magma: The Songxian syenite massif, Central China. Lithos, 2020, 366-367, 105554.	1.4	8
42	Fractional crystallization and magma mixing: evidence from porphyritic diorite-granodiorite dykes and mafic microgranular enclaves within the Zhoukoudian pluton, Beijing. Mineralogy and Petrology, 2014, 108, 777-800.	1.1	7
43	Geochronology, Geochemistry and Sr-Nd-Pb Isotopic Study of the Wulong Flower-Like Glomerophyric Diorite Porphyry (Central China): Implications for Tectonic Evolution of Eastern Qinling. Journal of Earth Science (Wuhan, China), 2018, 29, 1203-1218.	3.2	7
44	Partitioning of OH-F-Cl between biotite and silicate melt: Experiments and an empirical model. Geochimica Et Cosmochimica Acta, 2022, 317, 155-179.	3.9	7
45	Experimental investigation of reactions between two-mica granite and boron-rich fluids: Implications for the formation of tourmaline granite. Science China Earth Sciences, 2019, 62, 1630-1644.	5.2	6
46	Improvement of Electron Probe Microanalysis of Boron Concentration in Silicate Glasses. Microscopy and Microanalysis, 2019, 25, 874-882.	0.4	6
47	High-K calc-alkaline to shoshonitic intrusions in SE Tibet: implications for metasomatized lithospheric mantle beneath an active continental margin. Contributions To Mineralogy and Petrology, 2021, 176, 1.	3.1	5
48	Fluorine partitioning between titanite and silicate melt and its dependence on melt composition: experiments at 50–200 MPa and 875–925°C. European Journal of Mineralogy, 2018, 30, 33-44.	1.3	4
49	Anisotropic growth of La2NiO4+: Influential pre-treatment in molten-flux synthesis. Journal of Crystal Growth, 2019, 523, 125135.	1.5	4
50	Experimental evidence for a protracted enrichment of tungsten in evolving granitic melts: implications for scheelite mineralization. Mineralium Deposita, 2020, 55, 1299-1306.	4.1	4
51	"Origin of high-Mg adakitic magmatic enclaves from the Meichuan pluton, southern Dabie orogen (central China): Implications for delamination of the lower continental crust and melt-mantle interactionâ€â€"Reply. Lithos, 2011, 125, 839-844.	1.4	3
52	A flower-like glomerophyric diorite porphyry from Central China: Constraints on the unusual texture. Lithos, 2018, 318-319, 1-13.	1.4	3
53	Petrogenesis of deformed tourmaline leucogranite in the Gurla Mandhata metamorphic core complex, Southwestern Tibet. Lithos, 2020, 364-365, 105533.	1.4	3
54	In-situ U–Pb dating of zircon coronas, Sr–Nd–Hf isotopes and petrological constraints of the Daxigou anorthosite complex, NW China. Gondwana Research, 2022, 105, 96-116.	6.0	3

CHAO ZHANG

#	Article	IF	CITATIONS
55	Detrital zircon analysis of the Mesozoic strata in the northern Ordos Basin: Revealing the sourceâ€ŧoâ€sink relationships and tectonic settings. Geological Journal, 0, , .	1.3	2
56	Stabilizing Perovskite Structure by Interdiffusional Tailoring and Its Application in Composite Mixed Oxygen″onic and Electronic Conductors. Angewandte Chemie, 2017, 129, 7692-7696.	2.0	0
57	Magma Dynamics of Axial Melt Lens at Fastâ€Spreading Midâ€Ocean Ridges. Acta Geologica Sinica, 2020, 94, 80-80.	1.4	Ο
58	Partition of Ti between quartz and silicate melt. Reply to: Comment on Zhang et al., "Ti-in-quartz thermobarometry and TiO2 solubility in rhyolitic melts: New experiments and parametrization― Earth and Planetary Science Letters, 2021, 561, 116846.	4.4	0
59	On the improvement of calculating biotite formula from EPMA data: Reexamination of the methods of , , and reply to the discussion of Baidya and Das. Lithos, 2021, , 106403.	1.4	0